

CHORUS

This is the accepted manuscript made available via CHORUS. The article has been published as:

Measurements of Elliptic and Triangular Flow in High-Multiplicity $^3\text{He}+\text{Au}$ Collisions at $\sqrt{s_{\text{NN}}}=200$ GeV

A. Adare *et al.* (PHENIX Collaboration)

Phys. Rev. Lett. **115**, 142301 — Published 28 September 2015

DOI: [10.1103/PhysRevLett.115.142301](https://doi.org/10.1103/PhysRevLett.115.142301)

1 Measurements of elliptic and triangular flow in high-multiplicity $^3\text{He}+\text{Au}$ collisions at

$$\sqrt{s_{NN}} = 200 \text{ GeV}$$

3 A. Adare,¹⁴ S. Afanasiev,³³ C. Aidala,^{15,42,46,47} N.N. Ajitanand,⁶⁶ Y. Akiba,^{60,61} R. Akimoto,¹³ H. Al-Bataineh,⁵⁴
 4 J. Alexander,⁶⁶ M. Alfred,²⁶ H. Al-Ta'ani,⁵⁴ K.R. Andrews,¹ A. Angerami,¹⁵ K. Aoki,^{35,38,60} N. Apadula,^{31,67}
 5 L. Aphecetche,⁶⁸ E. Appelt,⁷² Y. Aramaki,^{13,60} R. Armendariz,^{9,54} S.H. Aronson,⁸ J. Asai,^{60,61} H. Asano,^{38,60}
 6 E.C. Aschenauer,⁸ E.T. Atomssa,^{39,67} R. Averbeck,⁶⁷ T.C. Awes,⁵⁶ B. Azmoun,⁸ V. Babintsev,²⁷ M. Bai,⁷
 7 G. Baksay,²¹ L. Baksay,²¹ A. Baldisseri,¹⁷ N.S. Bandara,⁴⁶ B. Bannier,⁶⁷ K.N. Barish,⁹ P.D. Barnes,^{42,*}
 8 B. Bassalleck,⁵³ A.T. Basye,¹ S. Bathe,^{6,9,61} S. Batsouli,⁵⁶ V. Baublis,⁵⁹ C. Baumann,^{8,48} A. Bazilevsky,⁸
 9 M. Beaumier,⁹ S. Beckman,¹⁴ S. Belikov,^{8,*} R. Belmont,^{47,72} J. Ben-Benjamin,⁴⁹ R. Bennett,⁶⁷ A. Berdnikov,⁶³
 10 Y. Berdnikov,⁶³ J.H. Bhom,⁷⁶ A.A. Bickley,¹⁴ D.S. Blau,³⁷ J.G. Boissevain,⁴² J.S. Bok,^{54,76} H. Borel,¹⁷
 11 K. Boyle,^{61,67} M.L. Brooks,⁴² D. Broxmeyer,⁴⁹ J. Bryslawskij,⁶ H. Buesching,⁸ V. Bumazhnov,²⁷ G. Bunce,^{8,61}
 12 S. Butsyk,^{42,67} C.M. Camacho,⁴² S. Campbell,^{15,31,67} A. Caringi,⁴⁹ P. Castera,⁶⁷ B.S. Chang,⁷⁶ W.C. Chang,²
 13 J.-L. Charvet,¹⁷ C.-H. Chen,^{61,67} S. Chernichenko,²⁷ C.Y. Chi,¹⁵ J. Chiba,³⁵ M. Chiu,^{8,28} I.J. Choi,^{28,76}
 14 J.B. Choi,¹¹ R.K. Choudhury,⁵ P. Christiansen,⁴⁴ T. Chujo,^{71,72} P. Chung,⁶⁶ A. Churny,²⁷ O. Chvala,⁹
 15 V. Cianciolo,⁵⁶ Z. Citron,^{67,74} C.R. Clevon,²³ B.A. Cole,¹⁵ M.P. Comets,⁵⁷ Z. Conesa del Valle,³⁹ M. Connors,⁶⁷
 16 P. Constantin,⁴² M. Csanád,¹⁹ T. Csörgő,⁷⁵ T. Dahms,⁶⁷ S. Dairaku,^{38,60} I. Danchev,⁷² D. Danley,⁵⁵ K. Das,²²
 17 A. Datta,^{46,53} M.S. Daugherty,¹ G. David,⁸ M.K. Dayananda,²³ M.B. Deaton,¹ K. DeBlasio,⁵³ K. Dehmelt,^{21,67}
 18 H. Delagrange,^{68,*} A. Denisov,²⁷ D. d'Enterria,^{15,39} A. Deshpande,^{61,67} E.J. Desmond,⁸ K.V. Dharmawardane,⁵⁴
 19 O. Dietzsch,⁶⁴ A. Dion,^{31,67} P.B. Diss,⁴⁵ J.H. Do,⁷⁶ M. Donadelli,⁶⁴ L. D'Orazio,⁴⁵ O. Drapier,³⁹ A. Drees,⁶⁷
 20 K.A. Drees,⁷ A.K. Dubey,⁷⁴ J.M. Durham,^{42,67} A. Durum,²⁷ D. Dutta,⁵ V. Dzhordzhadze,⁹ S. Edwards,^{7,22}
 21 Y.V. Efremenko,⁵⁶ J. Egdemir,⁶⁷ F. Ellinghaus,¹⁴ W.S. Emam,⁹ T. Engelmores,¹⁵ A. Enokizono,^{41,56,60,62}
 22 H. En'yo,^{60,61} S. Esumi,⁷¹ K.O. Eyser,^{8,9} B. Fadem,⁴⁹ N. Feege,⁶⁷ D.E. Fields,^{53,61} M. Finger,^{10,33}
 23 M. Finger, Jr.,^{10,33} F. Fleuret,³⁹ S.L. Fokin,³⁷ Z. Fraenkel,^{74,*} J.E. Frantz,^{55,67} A. Franz,⁸ A.D. Frawley,²²
 24 K. Fujiwara,⁶⁰ Y. Fukao,^{38,60} T. Fusayasu,⁵¹ S. Gadrat,⁴³ C. Gal,⁶⁷ P. Gallus,¹⁶ P. Garg,⁴ I. Garishvili,^{41,69}
 25 H. Ge,⁶⁷ F. Giordano,²⁸ A. Glenn,^{14,41} H. Gong,⁶⁷ X. Gong,⁶⁶ M. Gonin,³⁹ J. Gosset,¹⁷ Y. Goto,^{60,61}
 26 R. Granier de Cassagnac,³⁹ N. Grau,^{3,15,31} S.V. Greene,⁷² G. Grim,⁴² M. Grosse Perdekamp,^{28,61} Y. Gu,⁶⁷
 27 T. Gunji,¹³ L. Guo,⁴² H.-Å. Gustafsson,^{44,*} T. Hachiya,^{25,60} A. Hadj Henni,⁶⁸ C. Haegemann,⁵³ J.S. Haggerty,⁸
 28 K.I. Hahn,²⁰ H. Hamagaki,¹³ J. Hamblen,⁶⁹ H.F. Hamilton,¹ R. Han,⁵⁸ S.Y. Han,²⁰ J. Hanks,^{15,67} H. Harada,²⁵
 29 C. Harper,⁴⁹ E.P. Hartouni,⁴¹ K. Haruna,²⁵ S. Hasegawa,³² T.O.S. Haseler,²³ K. Hashimoto,^{60,62} E. Haslum,⁴⁴
 30 R. Hayano,¹³ X. He,²³ M. Heffner,⁴¹ T.K. Hemmick,⁶⁷ T. Hester,⁹ H. Hiejima,²⁸ J.C. Hill,³¹ R. Hobbs,⁵³
 31 M. Hohlmann,²¹ R.S. Hollis,⁹ W. Holzmann,^{15,66} K. Homma,²⁵ B. Hong,³⁶ T. Horaguchi,^{13,25,60,70,71} Y. Hori,¹³
 32 D. Hornback,^{56,69} T. Hoshino,²⁵ N. Hotvedt,³¹ J. Huang,⁸ S. Huang,⁷² T. Ichihara,^{60,61} R. Ichimiya,⁶⁰
 33 H. Iinuma,^{35,38,60} Y. Ikeda,⁷¹ K. Imai,^{32,38,60} J. Imrek,¹⁸ M. Inaba,⁷¹ Y. Inoue,^{60,62} A. Iordanova,⁹ D. Isenhower,¹
 34 L. Isenhower,¹ M. Ishihara,⁶⁰ T. Isobe,^{13,60} M. Issah,^{66,72} A. Isupov,³³ D. Ivanishchev,⁵⁹ Y. Iwanaga,²⁵
 35 B.V. Jacak,⁶⁷ M. Jezghani,²³ J. Jia,^{8,15,66} X. Jiang,⁴² J. Jin,¹⁵ O. Jinnouchi,⁶¹ D. John,⁶⁹ B.M. Johnson,⁸
 36 T. Jones,¹ K.S. Joo,⁵⁰ D. Jouan,⁵⁷ D.S. Jumper,^{1,28} F. Kajihara,¹³ S. Kametani,^{13,60,73} N. Kamihara,^{60,61}
 37 J. Kamin,⁶⁷ S. Kanda,¹³ M. Kaneta,⁶¹ S. Kaneti,⁶⁷ B.H. Kang,²⁴ J.H. Kang,⁷⁶ J.S. Kang,²⁴ H. Kanou,^{60,70}
 38 J. Kapustinsky,⁴² K. Karatsu,^{38,60} M. Kasai,^{60,62} D. Kawall,^{46,61} M. Kawashima,^{60,62} A.V. Kazantsev,³⁷
 39 T. Kempel,³¹ J.A. Key,⁵³ V. Khachatryan,⁶⁷ A. Khanzadeev,⁵⁹ K.M. Kijima,²⁵ J. Kikuchi,⁷³ A. Kim,²⁰ B.I. Kim,³⁶
 40 C. Kim,³⁶ D.H. Kim,⁵⁰ D.J. Kim,^{34,76} E. Kim,⁶⁵ E.-J. Kim,¹¹ G.W. Kim,²⁰ M. Kim,⁶⁵ S.H. Kim,⁷⁶ Y.-J. Kim,²⁸
 41 Y.K. Kim,²⁴ B. Kimelman,⁴⁹ E. Kinney,¹⁴ K. Kiriluk,¹⁴ Á. Kiss,¹⁹ E. Kistenev,⁸ R. Kitamura,¹³ A. Kiyomichi,⁶⁰
 42 J. Klatsky,²² J. Klay,⁴¹ C. Klein-Boesing,⁴⁸ D. Kleinjan,⁹ P. Kline,⁶⁷ T. Koblesky,¹⁴ L. Kochenda,⁵⁹
 43 V. Kochetkov,²⁷ B. Komkov,⁵⁹ M. Konno,⁷¹ J. Koster,²⁸ D. Kotchetkov,^{9,55} D. Kotov,^{59,63} A. Kozlov,⁷⁴ A. Král,¹⁶
 44 A. Kravitz,¹⁵ J. Kubart,^{10,30} G.J. Kunde,⁴² N. Kurihara,¹³ K. Kurita,^{60,62} M. Kurosawa,^{60,61} M.J. Kweon,³⁶
 45 Y. Kwon,^{69,76} G.S. Kyle,⁵⁴ R. Lacey,⁶⁶ Y.S. Lai,¹⁵ J.G. Lajoie,³¹ D. Layton,²⁸ A. Lebedev,³¹ D.M. Lee,⁴² J. Lee,²⁰
 46 K.B. Lee,³⁶ K.S. Lee,³⁶ M.K. Lee,⁷⁶ S. Lee,⁷⁶ S.H. Lee,⁶⁷ S.R. Lee,¹¹ T. Lee,⁶⁵ M.J. Leitch,⁴² M.A.L. Leite,⁶⁴
 47 B. Lenzi,⁶⁴ X. Li,¹² P. Lichtenwalner,⁴⁹ P. Liebing,⁶¹ S.H. Lim,⁷⁶ L.A. Linden Levy,¹⁴ T. Liška,¹⁶ A. Litvinenko,³³
 48 H. Liu,^{42,54} M.X. Liu,⁴² B. Love,⁷² D. Lynch,⁸ C.F. Maguire,⁷² Y.I. Makdisi,⁷ M. Makek,⁷⁷ A. Malakhov,³³
 49 M.D. Malik,⁵³ A. Manion,⁶⁷ V.I. Manko,³⁷ E. Mannel,^{8,15} Y. Mao,^{58,60} L. Mašek,^{10,30} H. Masui,⁷¹ F. Matathias,¹⁵
 50 M. McCumber,^{14,42,67} P.L. McGaughey,⁴² D. McGlinchey,^{14,22} C. McKinney,²⁸ N. Means,⁶⁷ A. Meles,⁵⁴

51 M. Mendoza,⁹ B. Meredith,²⁸ Y. Miake,⁷¹ T. Mibe,³⁵ A.C. Mignerey,⁴⁵ P. Mikeš,^{10,30} K. Miki,^{60,71} T.E. Miller,⁷²
 52 A. Milov,^{8,67,74} S. Mioduszewski,⁸ D.K. Mishra,⁵ M. Mishra,⁴ J.T. Mitchell,⁸ M. Mitrovski,⁶⁶ Y. Miyachi,^{60,70}
 53 S. Miyasaka,^{60,70} S. Mizuno,^{60,71} A.K. Mohanty,⁵ P. Montuenga,²⁸ H.J. Moon,⁵⁰ T. Moon,⁷⁶ Y. Morino,¹³
 54 A. Morreale,⁹ D.P. Morrison,^{8,†} S. Motschwiller,⁴⁹ T.V. Moukhanova,³⁷ D. Mukhopadhyay,⁷² T. Murakami,^{38,60}
 55 J. Murata,^{60,62} A. Mwai,⁶⁶ S. Nagamiya,^{35,60} K. Nagashima,²⁵ Y. Nagata,⁷¹ J.L. Nagle,^{14,‡} M. Naglis,⁷⁴
 56 M.I. Nagy,^{19,75} I. Nakagawa,^{60,61} H. Nakagomi,^{60,71} Y. Nakamiya,²⁵ K.R. Nakamura,^{38,60} T. Nakamura,^{25,60}
 57 K. Nakano,^{60,70} S. Nam,²⁰ C. Nattrass,⁶⁹ P.K. Netrakanti,⁵ J. Newby,⁴¹ M. Nguyen,⁶⁷ M. Nihashi,²⁵ T. Niida,⁷¹
 58 S. Nishimura,¹³ B.E. Norman,⁴² R. Nouicer,^{8,61} T. Novak,⁷⁵ N. Novitzky,^{34,67} A.S. Nyanin,³⁷ C. Oakley,²³
 59 E. O'Brien,⁸ S.X. Oda,¹³ C.A. Ogilvie,³¹ H. Ohnishi,⁶⁰ M. Oka,⁷¹ K. Okada,⁶¹ O.O. Omiwade,¹ Y. Onuki,⁶⁰
 60 J.D. Orjuela Koop,¹⁴ J.D. Osborn,⁴⁷ A. Oskarsson,⁴⁴ M. Ouchida,^{25,60} K. Ozawa,^{13,35} R. Pak,⁸ D. Pal,⁷²
 61 A.P.T. Palounek,⁴² V. Pantuev,^{29,67} V. Papavassiliou,⁵⁴ B.H. Park,²⁴ I.H. Park,²⁰ J. Park,⁶⁵ J.S. Park,⁶⁵
 62 S. Park,⁶⁵ S.K. Park,³⁶ W.J. Park,³⁶ S.F. Pate,⁵⁴ L. Patel,²³ M. Patel,³¹ H. Pei,³¹ J.-C. Peng,²⁸ H. Pereira,¹⁷
 63 D.V. Perepelitsa,⁸ G.D.N. Perera,⁵⁴ V. Peresedov,³³ D.Yu. Peressounko,³⁷ J. Perry,³¹ R. Petti,^{8,67}
 64 C. Pinkenburg,⁸ R. Pinson,¹ R.P. Pisani,⁸ M. Proissl,⁶⁷ M.L. Purschke,⁸ A.K. Purwar,⁴² H. Qu,²³ J. Rak,^{34,53}
 65 A. Rakotozafindrabe,³⁹ B.J. Ramson,⁴⁷ I. Ravinovich,⁷⁴ K.F. Read,^{56,69} S. Rembeczki,²¹ M. Reuter,⁶⁷ K. Reygers,⁴⁸
 66 D. Reynolds,⁶⁶ V. Riabov,^{52,59} Y. Riabov,^{59,63} E. Richardson,⁴⁵ T. Rinn,³¹ D. Roach,⁷² G. Roche,^{43,*}
 67 S.D. Rolnick,⁹ A. Romana,^{39,*} M. Rosati,³¹ C.A. Rosen,¹⁴ S.S.E. Rosendahl,⁴⁴ P. Rosnet,⁴³ Z. Rowan,⁶
 68 J.G. Rubin,⁴⁷ P. Rukoyatkin,³³ P. Ružička,³⁰ V.L. Rykov,⁶⁰ B. Sahlmueller,^{48,67} N. Saito,^{35,38,60,61} T. Sakaguchi,⁸
 69 S. Sakai,⁷¹ K. Sakashita,^{60,70} H. Sakata,²⁵ H. Sako,³² V. Samsonov,^{52,59} S. Sano,^{13,73} M. Sarsour,²³ S. Sato,^{32,35}
 70 T. Sato,⁷¹ M. Savastio,⁶⁷ S. Sawada,³⁵ B. Schaefer,⁷² B.K. Schmoll,⁶⁹ K. Sedgwick,⁹ J. Seele,¹⁴ R. Seidl,^{28,60,61}
 71 A.Yu. Semenov,³¹ V. Semenov,^{27,29} A. Sen,^{23,69} R. Seto,⁹ P. Sett,⁵ A. Sexton,⁴⁵ D. Sharma,^{67,74} I. Shein,²⁷
 72 A. Shevel,^{59,66} T.-A. Shibata,^{60,70} K. Shigaki,²⁵ H.H. Shim,³⁶ M. Shimomura,^{31,71} K. Shoji,^{38,60} P. Shukla,⁵
 73 A. Sickles,^{8,28,67} C.L. Silva,^{31,42,64} D. Silvermyr,^{44,56} C. Silvestre,¹⁷ K.S. Sim,³⁶ B.K. Singh,⁴ C.P. Singh,⁴
 74 V. Singh,⁴ S. Skutnik,³¹ M. Slunečka,^{10,33} M. Snowball,⁴² T. Sodre,⁴⁹ A. Soldatov,²⁷ R.A. Soltz,⁴¹ W.E. Sondheim,⁴²
 75 S.P. Sorensen,⁶⁹ I.V. Sourikova,⁸ F. Staley,¹⁷ P.W. Stankus,⁵⁶ E. Stenlund,⁴⁴ M. Stepanov,^{46,*} A. Ster,⁷⁵
 76 S.P. Stoll,⁸ T. Sugitate,²⁵ C. Suire,⁵⁷ A. Sukhanov,⁸ T. Sumita,⁶⁰ J. Sun,⁶⁷ J. Sziklai,⁷⁵ T. Tabaru,⁶¹ S. Takagi,⁷¹
 77 E.M. Takagui,⁶⁴ A. Takahara,¹³ A. Taketani,^{60,61} R. Tanabe,⁷¹ Y. Tanaka,⁵¹ S. Taneja,⁶⁷ K. Tanida,^{38,60,61,65}
 78 M.J. Tannenbaum,⁸ S. Tarafdar,^{4,74} A. Taranenko,^{52,66} P. Tarján,¹⁸ E. Tennant,⁵⁴ H. Themann,⁶⁷ D. Thomas,¹
 79 T.L. Thomas,⁵³ R. Tieulent,²³ A. Timilsina,³¹ T. Todoroki,^{60,71} M. Togawa,^{38,60,61} A. Toia,⁶⁷ J. Tojo,⁶⁰
 80 L. Tomášek,³⁰ M. Tomášek,^{16,30} Y. Tomita,⁷¹ H. Torii,^{25,60} C.L. Towell,¹ R. Towell,¹ R.S. Towell,¹
 81 V.-N. Tram,³⁹ I. Tserruya,⁷⁴ Y. Tsuchimoto,²⁵ K. Utsunomiya,¹³ C. Vale,^{8,31} H. Valle,⁷² H.W. van Hecke,⁴²
 82 E. Vazquez-Zambrano,¹⁵ A. Veicht,^{15,28} J. Velkovska,⁷² R. Vértesi,^{18,75} A.A. Vinogradov,³⁷ M. Virius,¹⁶
 83 A. Vossen,²⁸ V. Vrba,^{16,30} E. Vznuzdaev,⁵⁹ M. Wagner,^{38,60} D. Walker,⁶⁷ X.R. Wang,^{54,61} D. Watanabe,²⁵
 84 K. Watanabe,⁷¹ Y. Watanabe,^{60,61} Y.S. Watanabe,^{13,35} F. Wei,^{31,54} R. Wei,⁶⁶ J. Wessels,⁴⁸ A.S. White,⁴⁷
 85 S.N. White,⁸ D. Winter,¹⁵ C.L. Woody,⁸ R.M. Wright,¹ M. Wysocki,^{14,56} B. Xia,⁵⁵ W. Xie,⁶¹ L. Xue,²³ S. Yalcin,⁶⁷
 86 Y.L. Yamaguchi,^{13,60,67,73} K. Yamaura,²⁵ R. Yang,²⁸ A. Yanovich,²⁷ Z. Yasin,⁹ J. Ying,²³ S. Yokkaichi,^{60,61}
 87 J.H. Yoo,³⁶ J.S. Yoo,²⁰ I. Yoon,⁶⁵ Z. You,^{42,58} G.R. Young,⁵⁶ I. Younus,^{40,53} H. Yu,⁵⁸ I.E. Yushmanov,³⁷
 88 W.A. Zajc,¹⁵ O. Zaudtke,⁴⁸ A. Zelenski,⁷ C. Zhang,⁵⁶ S. Zhou,¹² J. Zimanyi,^{75,*} L. Zolin,³³ and L. Zou⁹

(PHENIX Collaboration)

¹Abilene Christian University, Abilene, Texas 79699, USA

²Institute of Physics, Academia Sinica, Taipei 11529, Taiwan

³Department of Physics, Augustana College, Sioux Falls, South Dakota 57197, USA

⁴Department of Physics, Banaras Hindu University, Varanasi 221005, India

⁵Bhabha Atomic Research Centre, Bombay 400 085, India

⁶Baruch College, City University of New York, New York, New York, 10010 USA

⁷Collider-Accelerator Department, Brookhaven National Laboratory, Upton, New York 11973-5000, USA

⁸Physics Department, Brookhaven National Laboratory, Upton, New York 11973-5000, USA

⁹University of California-Riverside, Riverside, California 92521, USA

¹⁰Charles University, Ovocný trh 5, Praha 1, 116 36, Prague, Czech Republic

¹¹Chonbuk National University, Jeonju, 561-756, Korea

¹²Science and Technology on Nuclear Data Laboratory, China Institute of Atomic Energy, Beijing 102413, P. R. China

¹³Center for Nuclear Study, Graduate School of Science, University of Tokyo, 7-3-1 Hongo, Bunkyo, Tokyo 113-0033, Japan

¹⁴University of Colorado, Boulder, Colorado 80309, USA

¹⁵Columbia University, New York, New York 10027 and Nevis Laboratories, Irvington, New York 10533, USA

- 105 ¹⁶ Czech Technical University, Zikova 4, 166 36 Prague 6, Czech Republic
 106 ¹⁷ Dapnia, CEA Saclay, F-91191, Gif-sur-Yvette, France
 107 ¹⁸ Debrecen University, H-4010 Debrecen, Egyetem tér 1, Hungary
 108 ¹⁹ ELTE, Eötvös Loránd University, H-1117 Budapest, Pázmány P. s. 1/A, Hungary
 109 ²⁰ Ewha Womans University, Seoul 120-750, Korea
 110 ²¹ Florida Institute of Technology, Melbourne, Florida 32901, USA
 111 ²² Florida State University, Tallahassee, Florida 32306, USA
 112 ²³ Georgia State University, Atlanta, Georgia 30303, USA
 113 ²⁴ Hanyang University, Seoul 133-792, Korea
 114 ²⁵ Hiroshima University, Kagamiyama, Higashi-Hiroshima 739-8526, Japan
 115 ²⁶ Department of Physics and Astronomy, Howard University, Washington, DC 20059, USA
 116 ²⁷ IHEP Protvino, State Research Center of Russian Federation, Institute for High Energy Physics, Protvino, 142281, Russia
 117 ²⁸ University of Illinois at Urbana-Champaign, Urbana, Illinois 61801, USA
 118 ²⁹ Institute for Nuclear Research of the Russian Academy of Sciences, prospekt 60-letiya Oktyabrya 7a, Moscow 117312, Russia
 119 ³⁰ Institute of Physics, Academy of Sciences of the Czech Republic, Na Slovance 2, 182 21 Prague 8, Czech Republic
 120 ³¹ Iowa State University, Ames, Iowa 50011, USA
 121 ³² Advanced Science Research Center, Japan Atomic Energy Agency, 2-4
 122 Shirakata Shirane, Tokai-mura, Naka-gun, Ibaraki-ken 319-1195, Japan
 123 ³³ Joint Institute for Nuclear Research, 141980 Dubna, Moscow Region, Russia
 124 ³⁴ Helsinki Institute of Physics and University of Jyväskylä, P.O.Box 35, FI-40014 Jyväskylä, Finland
 125 ³⁵ KEK, High Energy Accelerator Research Organization, Tsukuba, Ibaraki 305-0801, Japan
 126 ³⁶ Korea University, Seoul, 136-701, Korea
 127 ³⁷ Russian Research Center “Kurchatov Institute”, Moscow, 123098 Russia
 128 ³⁸ Kyoto University, Kyoto 606-8502, Japan
 129 ³⁹ Laboratoire Leprince-Ringuet, Ecole Polytechnique, CNRS-IN2P3, Route de Saclay, F-91128, Palaiseau, France
 130 ⁴⁰ Physics Department, Lahore University of Management Sciences, Lahore 54792, Pakistan
 131 ⁴¹ Lawrence Livermore National Laboratory, Livermore, California 94550, USA
 132 ⁴² Los Alamos National Laboratory, Los Alamos, New Mexico 87545, USA
 133 ⁴³ LPC, Université Blaise Pascal, CNRS-IN2P3, Clermont-Fd, 63177 Aubiere Cedex, France
 134 ⁴⁴ Department of Physics, Lund University, Box 118, SE-221 00 Lund, Sweden
 135 ⁴⁵ University of Maryland, College Park, Maryland 20742, USA
 136 ⁴⁶ Department of Physics, University of Massachusetts, Amherst, Massachusetts 01003-9337, USA
 137 ⁴⁷ Department of Physics, University of Michigan, Ann Arbor, Michigan 48109-1040, USA
 138 ⁴⁸ Institut für Kernphysik, University of Muenster, D-48149 Muenster, Germany
 139 ⁴⁹ Muhlenberg College, Allentown, Pennsylvania 18104-5586, USA
 140 ⁵⁰ Myongji University, Yongin, Kyonggido 449-728, Korea
 141 ⁵¹ Nagasaki Institute of Applied Science, Nagasaki-shi, Nagasaki 851-0193, Japan
 142 ⁵² National Research Nuclear University, MEPhI, Moscow Engineering Physics Institute, Moscow, 115409, Russia
 143 ⁵³ University of New Mexico, Albuquerque, New Mexico 87131, USA
 144 ⁵⁴ New Mexico State University, Las Cruces, New Mexico 88003, USA
 145 ⁵⁵ Department of Physics and Astronomy, Ohio University, Athens, Ohio 45701, USA
 146 ⁵⁶ Oak Ridge National Laboratory, Oak Ridge, Tennessee 37831, USA
 147 ⁵⁷ IPN-Orsay, Université Paris Sud, CNRS-IN2P3, BP1, F-91406, Orsay, France
 148 ⁵⁸ Peking University, Beijing 100871, P. R. China
 149 ⁵⁹ PNPI, Petersburg Nuclear Physics Institute, Gatchina, Leningrad region, 188300, Russia
 150 ⁶⁰ RIKEN Nishina Center for Accelerator-Based Science, Wako, Saitama 351-0198, Japan
 151 ⁶¹ RIKEN BNL Research Center, Brookhaven National Laboratory, Upton, New York 11973-5000, USA
 152 ⁶² Physics Department, Rikkyo University, 3-34-1 Nishi-Ikebukuro, Toshima, Tokyo 171-8501, Japan
 153 ⁶³ Saint Petersburg State Polytechnic University, St. Petersburg, 195251 Russia
 154 ⁶⁴ Universidade de São Paulo, Instituto de Física, Caixa Postal 66318, São Paulo CEP05315-970, Brazil
 155 ⁶⁵ Department of Physics and Astronomy, Seoul National University, Seoul 151-742, Korea
 156 ⁶⁶ Chemistry Department, Stony Brook University, SUNY, Stony Brook, New York 11794-3400, USA
 157 ⁶⁷ Department of Physics and Astronomy, Stony Brook University, SUNY, Stony Brook, New York 11794-3800, USA
 158 ⁶⁸ SUBATECH (Ecole des Mines de Nantes, CNRS-IN2P3, Université de Nantes) BP 20722-44307, Nantes, France
 159 ⁶⁹ University of Tennessee, Knoxville, Tennessee 37996, USA
 160 ⁷⁰ Department of Physics, Tokyo Institute of Technology, Oh-okayama, Meguro, Tokyo 152-8551, Japan
 161 ⁷¹ Institute of Physics, University of Tsukuba, Tsukuba, Ibaraki 305, Japan
 162 ⁷² Vanderbilt University, Nashville, Tennessee 37235, USA
 163 ⁷³ Waseda University, Advanced Research Institute for Science and
 164 Engineering, 17 Kikui-cho, Shinjuku-ku, Tokyo 162-0044, Japan
 165 ⁷⁴ Weizmann Institute, Rehovot 76100, Israel
 166 ⁷⁵ Institute for Particle and Nuclear Physics, Wigner Research Centre for Physics, Hungarian
 167 Academy of Sciences (Wigner RCP, RMKI) H-1525 Budapest 114, POBox 49, Budapest, Hungary
 168 ⁷⁶ Yonsei University, IPAP, Seoul 120-749, Korea

⁷⁷University of Zagreb, Faculty of Science, Department of Physics, Bijenička 32, HR-10002 Zagreb, Croatia

(Dated: September 22, 2015)

We present the first measurement of elliptic (v_2) and triangular (v_3) flow in high-multiplicity $^3\text{He}+\text{Au}$ collisions at $\sqrt{s_{NN}} = 200$ GeV. Two-particle correlations, where the particles have a large separation in pseudorapidity, are compared in $^3\text{He}+\text{Au}$ and in $p+p$ collisions and indicate that collective effects dominate the second and third Fourier components for the correlations observed in the $^3\text{He}+\text{Au}$ system. The collective behavior is quantified in terms of elliptic v_2 and triangular v_3 anisotropy coefficients measured with respect to their corresponding event planes. The v_2 values are comparable to those previously measured in $d+\text{Au}$ collisions at the same nucleon-nucleon center-of-mass energy. Comparison with various theoretical predictions are made, including to models where the hot spots created by the impact of the three ^3He nucleons on the Au nucleus expand hydrodynamically to generate the triangular flow. The agreement of these models with data may indicate the formation of low-viscosity quark-gluon plasma even in these small collision systems.

PACS numbers: 25.75.Dw

The study of high-energy heavy ion collisions at the Relativistic Heavy Ion Collider (RHIC) and the Large Hadron Collider has produced abundant evidence for the formation of Quark-Gluon Plasma (QGP). Observation of strong elliptic and triangular flow in these $A+A$ collisions indicates that the QGP has very small viscosity and behaves like a nearly perfect fluid [1–3]. Recently, measurements at the large hadron collider in very high multiplicity events from collisions of $p+p$ and $p+Pb$ have revealed similar particle emission patterns [4–8]. Such features have also been detected in $d+Au$ collisions at RHIC [9–11]. Explanations of the data in terms of the formation of small droplets of QGP which then expand hydrodynamically [12] compete with alternatives involving novel initial-state effects (e.g. glasma models [13]). RHIC is uniquely suited to test these competing theories by its ability to engineer the size and shape of the initial reaction zone through collisions of $p+Au$, $d+Au$, and $^3\text{He}+Au$, as proposed in Ref. [14]. In the case when small QGP droplets are formed, the latter two systems should have the strongest elliptic and triangular flow patterns, respectively.

The azimuthal anisotropy of produced particles can be quantified by the Fourier coefficients v_n in the expansion of the particles' distribution as: $dN/d\phi \propto 1 + \sum_{n=1} 2v_n \cos(n(\phi - \Psi_n))$ [15], where n is the order of the harmonic, ϕ is the azimuthal angle of particles of a given type, and Ψ_n is the azimuthal angle of the n th-order event plane. In this Letter, the elliptic (v_2) and triangular (v_3) flow for inclusive charged hadrons produced at midrapidity $|\eta| < 0.35$ in high-multiplicity $^3\text{He}+Au$ collisions at $\sqrt{s_{NN}} = 200$ GeV are measured in the PHENIX experiment with respect to Ψ_2 and Ψ_3 event planes. The signatures of collective motion beyond known nonflow correlation effects (e.g. jets, resonances, etc.) are also examined by comparing long-range correlations between $^3\text{He}+Au$ and $p+p$ collisions.

A full description of the PHENIX experimental setup is given in Ref. [16]. Charged particles are reconstructed in the two PHENIX central-arm tracking systems comprising drift chambers and multi-wire proportional pad chambers (PC) [17]. Each arm covers $\pi/2$ in azimuth and $|\eta| < 0.35$. The drift-chamber tracks are matched to hits in the outermost PC layer (PC3), reducing the contribution of tracks originating from decays and photon conversions.

The observed event-plane angles Ψ_n^{Obs} are measured in different pseudorapidity ranges by the beam-beam counters [18] (BBC) and forward-silicon-vertex [19] (FVTX) detectors. The PHENIX experiment has two BBCs, each comprising 64 quartz Čerenkov radiators read out by photomultiplier tubes (PMTs), subtending pseudorapidity ($3.0 < |\eta| < 3.9$). The FVTX [19] detector comprises two identical endcap assemblies, located symmetrically in the north and south directions. Charged particles can be detected with a high efficiency ($> 95\%$) using a cluster of mini-strip hits. The event planes are measured by the BBC in the Au-going (south) direction (BBC-S), which covers $-3.9 < \eta < -3.0$, and by the reconstructed clusters in the FVTX in the Au-going (south) endcap (FVTX-S), which covers $-3.0 < \eta < -1.0$.

The $^3\text{He}+Au$ data for this analysis were obtained in the 2014 run of the PHENIX experiment and include 1.6 billion minimum-bias (MB) triggered events and 480 million high-multiplicity (HM) triggered events. The MB trigger is defined as a coincidence between the north and south BBCs requiring one or more photomultiplier tubes firing in each, capturing $88 \pm 4\%$ of the total inelastic $^3\text{He}+Au$ cross section. The HM trigger is based on the MB trigger, but additionally requires more than 48 photomultiplier tubes firing in the BBC-S.

The event centrality class in $^3\text{He}+Au$ collisions is determined as a percentile of the total charge $\sum Q^{\text{BBC-S}}$ measured in the BBC-S [18, 20–22]. The distribution of BBC-S PMT charge sum is shown in Fig. 1 for both MB and HM triggered events. The distribution for HM events has been scaled down by the relative online trigger prescale factor. For the MB sample, a threshold on the BBC-S charge sum shown in Fig. 1 is applied to select the top 5% central $^3\text{He}+Au$ collisions. In total, 400 million events have been used for the measurement of v_2 and v_3 including both HM and MB triggered events having BBC-S charge sum above the threshold.

Events with high BBC-S sum charge have been simulated with a Monte Carlo Glauber model [23, 24], following the procedure detailed in Ref. [18]. The average number of binary collisions (N_{coll}), participants (N_{part}) and initial-state eccentricities (ε_2 , ε_3) were found to be consistent, within uncertainties, between the MB with the 0%–5% central selection, and the HM events being used here. Note that in this Glauber calculation the spatial distribution from each participant is smeared with a two-dimensional Gaussian, $\sigma_r = 0.4$ fm [18]. The simulation results for central $^3\text{He}+Au$ and $d+Au$ are listed in Table I with the $d+Au$ values from Ref. [18].

TABLE I. Monte Carlo Glauber characterization results.

System	N_{part}	N_{coll}	ε_2	ε_3
0%–5% $^3\text{He}+Au$	25.0 ± 1.6	26.1 ± 2.0	0.50 ± 0.02	0.28 ± 0.02
0%–5% $d+Au$	17.3 ± 1.2	18.1 ± 1.2	0.54 ± 0.04	0.19 ± 0.01

To estimate the contribution to the flow measurements from elementary processes, such as jets and resonance

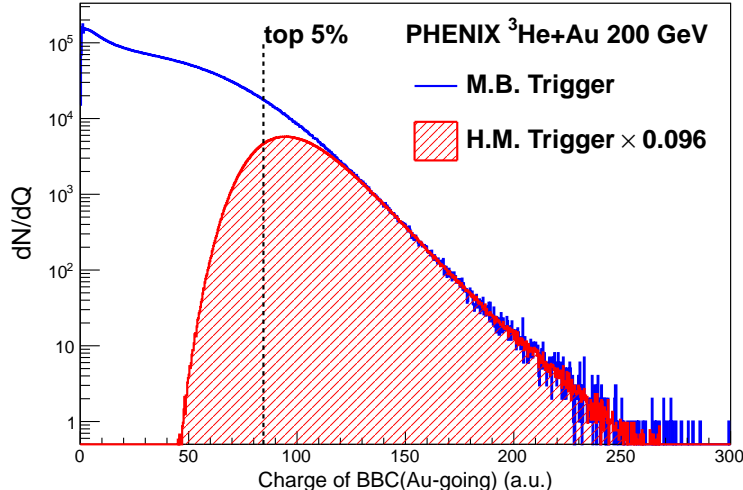


FIG. 1. (Color online) The BBC-S charge distribution in minimum bias ${}^3\text{He}+\text{Au}$ events and in high-multiplicity triggered events, scaled appropriately. The dashed line indicates the threshold selecting the 0%–5% most central events.

220 decay, we first examine azimuthal correlations in minimum bias $p+p$ and central ${}^3\text{He}+\text{Au}$ events across a long range
 221 in pseudorapidity, with $|\Delta\eta| \sim 3.5$ between tracks in the PHENIX central arm at a given p_T and charge measured in
 222 the BBC PMTs. We use the BBCs for these correlation functions because the detector configuration and performance
 223 is uniform over many years, which enables us to combine data for $p+p$ collisions at $\sqrt{s} = 200$ GeV from running in
 224 2005, 2006, 2008, and 2009. This results in 2.7 billion total minimum bias $p+p$ events.

225 Using track-BBC pairs we construct the distribution over relative azimuth, and from that the normalized correlation
 226 function:

$$S(\Delta\phi, p_T) = \frac{d(w_{\text{PMT}} N_{\text{Same event}}^{\text{track}(p_T)-\text{PMT}})}{d\Delta\phi} \quad (1)$$

$$C(\Delta\phi, p_T) = \frac{S(\Delta\phi, p_T)}{M(\Delta\phi, p_T)} \frac{\int_0^{2\pi} M(\Delta\phi, p_T) d\Delta\phi}{\int_0^{2\pi} S(\Delta\phi, p_T) d\Delta\phi} \quad (2)$$

227 The weighting w_{PMT} for each pair is taken as the PMT charge. The signal distribution S is over pairs in the same
 228 event; the mixed distribution M is over pairs from different events in the same event centrality and z vertex bin, and
 229 serves to correct for any nonuniformity in acceptance over $\Delta\phi$.

230 Figure 2 shows the correlation functions $C(\Delta\phi, p_T)$ for different p_T bins, for HM ${}^3\text{He}+\text{Au}$ collisions using (a)–
 231 (c) BBC-S and (d)–(f) minimum bias $p+p$ collisions using both BBCs. We analyze these shapes by fitting each
 232 $C(\Delta\phi, p_T)$ to a four-term Fourier cosine expansion, $f(\Delta\phi) = 1 + \sum_{n=1}^4 2c_n(p_T) \cos(n\Delta\phi)$. The sum function and
 233 each individual cosine component are plotted in Fig. 2 for each distribution. Central ${}^3\text{He}+\text{Au}$ collisions show a clearly
 234 visible enhancement of near-side pairs, producing a local maximum in the distribution at $\Delta\phi \sim 0$. In contrast, $p+p$
 235 collisions can be described almost completely by the dipole term $\cos(\Delta\phi)$, as expected generically from back-to-back
 236 jets and transverse momentum conservation.

As in our $d+\text{Au}$ analysis [10], we estimate quantitatively the correlation strength that would be observed in a
 class of ${}^3\text{He}+\text{Au}$ collisions purely from elementary processes, such as in $p+p$ collisions. Approximating the ${}^3\text{He}+\text{Au}$
 collisions as superpositions of some number N of $p+p$ collisions, we would then expect the correlation strengths c_n
 from the superposition to be the same as in $p+p$, but diluted by a factor of $1/N$. We then approximate this dilution
 factor as simply the ratio of total charge observed in the BBC-S detector in $p+p$ versus ${}^3\text{He}+\text{Au}$:

$$c_n^{\text{HeAu elementary}}(p_T) \simeq c_n^{p+p}(p_T) \frac{(\sum Q^{\text{BBC-S}})_{p+p}}{(\sum Q^{\text{BBC-S}})_{\text{HeAu}}} \quad (3)$$

237 with a numerical value of $1/(20.6 \pm 0.4)$. Figure 3(a) shows the c_n 's from the ${}^3\text{He}+\text{Au}$ correlation functions, and from
 238 the $p+p$ with the dilution factor applied. The c_2^{pp} is found to be positive and the c_3^{pp} to be negative. This indicates

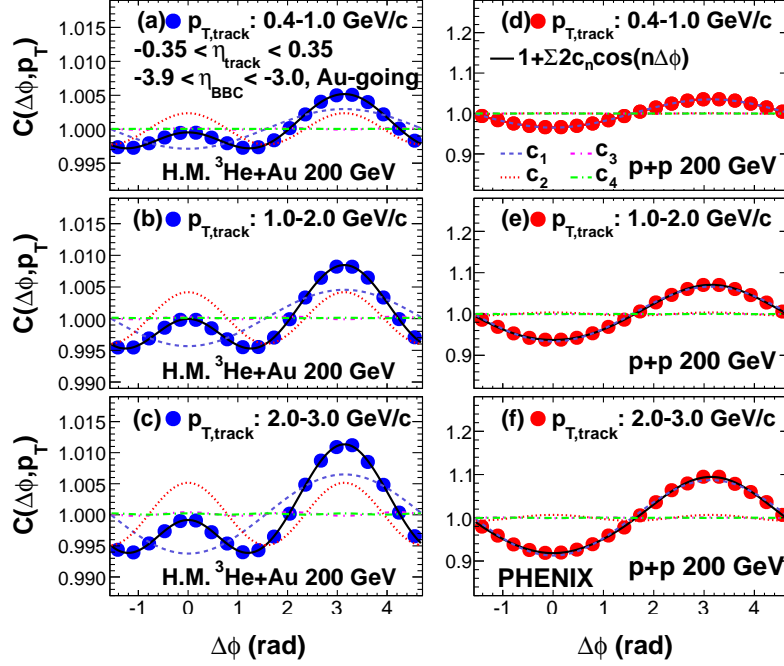


FIG. 2. (Color online) The azimuthal correlation functions $C(\Delta\phi, p_T)$, as defined in Eq. 2, for track-BBC pairs with different track p_T selections in (a)–(c) HM ${}^3\text{He}+\text{Au}$ collisions and (d)–(f) minimum bias $p+p$ collisions both at $\sqrt{s_{NN}} = 200$ GeV. The track p_T bins are (a),(d) 0.4–1.0, (b),(e) 1.0–2.0, and (c),(f) 2.0–3.0 GeV/c. Each correlation function is fit with a four-term Fourier cosine expansion; the individual components $n = 1$ to $n = 4$ are drawn on each panel, together with the fit function sum.

239 that the correlation of elementary processes contributes positively to the v_2 but negatively to the v_3 . The ratios in
 240 Fig. 3(b) show that the relative correlation strength in ${}^3\text{He}+\text{Au}$ from elementary processes grows with p_T , as might
 241 be expected from jet processes for example, but does not exceed 7% (15%) for c_2 (c_3).

242 We now quantify the strength of collective behavior through the v_n coefficients. The v_n coefficients for charged
 243 hadrons at midrapidity are measured in central ${}^3\text{He}+\text{Au}$ events via the event-plane method [25] as $v_n(p_T) =$
 244 $\langle \cos n(\phi^{\text{Particle}}(p_T) - \Psi_n^{\text{Obs}}) \rangle / \text{Res}(\Psi_n^{\text{Obs}})$, where the average is over particles in the same p_T bin and events of the
 245 same centrality. The n th-order event-plane direction Ψ_n^{Obs} is determined in each event with the BBC-S or FVTX-S
 246 detectors. The Ψ_n^{Obs} are corrected for each detector with a standard event-plane flattening technique [25–28] to remove
 247 the effect of any small, residual nonuniformities in the detector response. As a cross-check we use event planes from
 248 both the full FVTX-S covering $-3.0 < \eta < -1.0$ and a subsection covering $-2.5 < \eta < -1.5$. The choice of the latter
 249 is to avoid edge effects and still retain good FVTX-S acceptance.

250 We calculate the resolutions $\text{Res}(\Psi_n^{\text{Obs}})$ for each detector at each n using the standard three-event-plane method [10,
 251 25], combining two event planes with the n th order event plane determined from central-arm tracks, restricted to low
 252 p_T ($0.2 < p_T < 2.0$ GeV/c) to minimize contribution from jet fragments. In the case of the $n = 2$ event plane,
 253 the resolution is also estimated using the first-order event plane measured with spectator neutrons in the shower-
 254 maximum detector of the zero-degree calorimeter [28, 29] on the Au-going side ($\eta < -6.5$). The values for the
 255 resolution obtained in both methods are found to be consistent within uncertainties.

256 The event plane resolutions for each detector and order are shown in Table II. The v_2 and v_3 measured using the
 257 three event planes described above are shown in Fig. 3(c), and are consistent between detectors to within 5%(15%)
 258 for v_2 (v_3) over the whole p_T range.

259 The main sources of systematic uncertainty for the v_n measurements are: (1) track backgrounds from weak decays
 260 and photon conversions; (2) multiple ${}^3\text{He}+\text{Au}$ collisions in a bunch crossing (pile-up); (3) biases in event plane
 261 determination; (4) the effect of detector alignment and performance on the v_n measurement; and (5) elementary
 262 process/nonflow correlations. We assign the following values to account for these systematic uncertainties: (1) We
 263 estimate the track background contribution by reducing the spatial matching windows in PC3 from 3σ to 2σ , and find
 264 a change of less than 2%(5%) fractionally in v_2 (v_3). (2) We expect the v_n from pile-up events to be modestly reduced.
 265 Conservatively assuming that pile-up events that contaminate the sample at the level of 4%–5% have a negligible

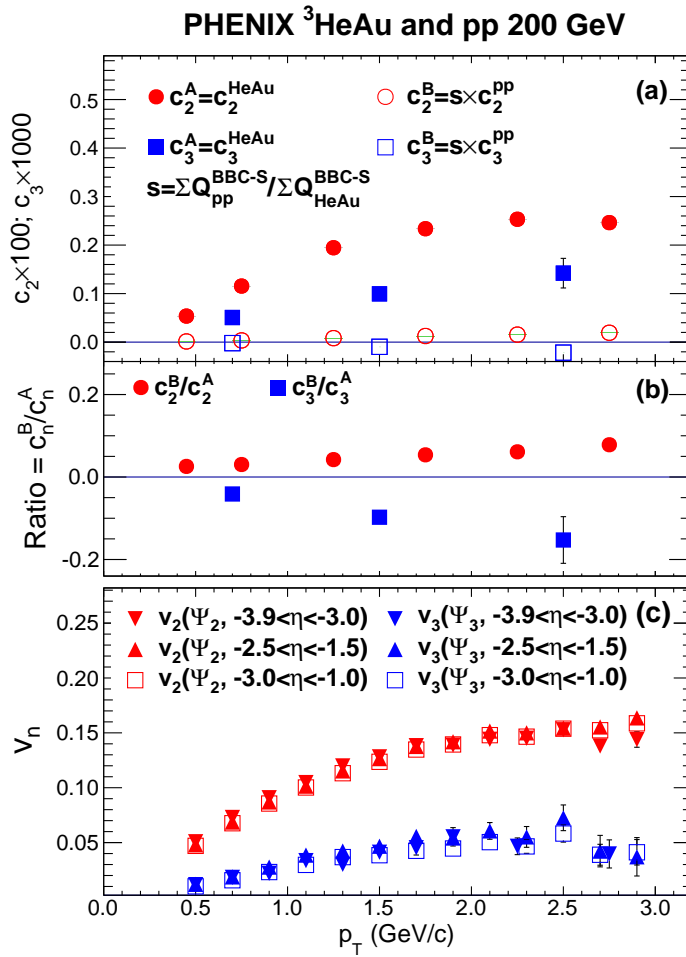


FIG. 3. (Color online) (a) The $c_n(p_T)$ coefficients for track-BBC pairs from high multiplicity ${}^3\text{HeAu}$ collisions (filled, denoted “ c^A ”) and $c_n(p_T)$ for pairs in minimum bias $p+p$ collisions times the dilution factor $(\sum Q^{\text{BBC-S}})_{p+p} / (\sum Q^{\text{BBC-S}})_{\text{HeAu}}$ (open, denoted “ c^B ”). (b) The ratio c^B/c^A is shown with statistical error bars. (c) Comparison of extracted values of v_2 and v_3 for midrapidity tracks in central ${}^3\text{HeAu}$ using event plane measurements with detectors in different pseudorapidity intervals (see text).

TABLE II. The resolution of n th-order event-plane angles measured by the BBC-S and FVTX-S detectors.

Subsystem	$\text{Res}(\Psi_2^{\text{Obs}})$	$\text{Res}(\Psi_3^{\text{Obs}})$
BBC-S ($-3.9 < \eta < -3.0$)	0.110	0.034
FVTX-S ($-2.5 < \eta < -1.5$)	0.232	0.052
FVTX-S ($-3.0 < \eta < -1.0$)	0.274	0.070

266 v_n , this results in a $\pm 5\%$ systematic uncertainty. (3) Event plane effects are estimated from v_n measurements using
 267 different event plane detectors as shown in Fig. 3(c). They are no more than 5%(15%) for $v_2(v_3)$. (4) The difference of
 268 v_n for charged hadrons measured by the east and west DC arms are found to be less than 2%(15%) for $v_2(v_3)$. (5) The
 269 contribution from nonflow correlations at each p_T is estimated from Fig. 3(b), reaching a maximum of 7%(15%) for
 270 $v_2(v_3)$. We do not attempt to correct for this contribution and instead treat it as a systematic uncertainty. All of
 271 these contributions are summed in quadrature.

272 The final v_n results are determined using the event plane measured in the FVTX-S covering $-3.0 < \eta < -1.0$, and these
 273 are shown in Fig. 4, with the systematic uncertainties as described above. We observe sizable v_2 and v_3 anisotropies
 274 that both rise as a function of p_T . It is notable that the $v_2(p_T)$ values for central ${}^3\text{HeAu}$ collisions are very similar

275 within uncertainties with those reported earlier in central $d+Au$ collisions [10]. In scenarios where these anisotropies
 276 reflect the initial geometry, this similarity would be expected as the initial eccentricities ε_2 for central $d+Au$ and
 277 ${}^3\text{He}+Au$ are essentially identical, as shown in Table I. The same calculations indicate a much larger ε_3 in ${}^3\text{He}+Au$
 278 compared with $d+Au$ collisions. However, the $d+Au$ data used in [10] were taken in 2008, without a central trigger
 279 and before the FVTX was installed, and did not allow extraction of a statistically significant v_3 in $d+Au$.

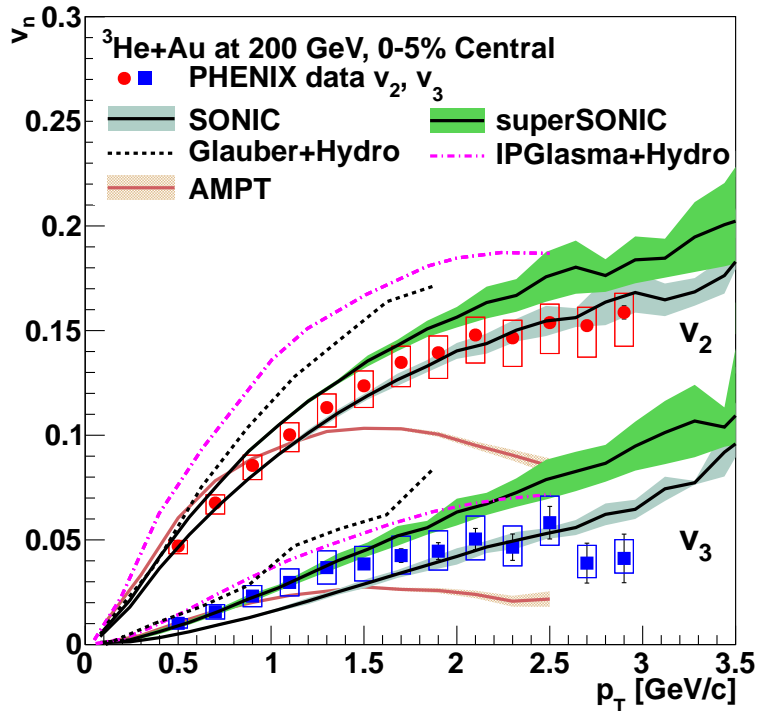


FIG. 4. (Color online) Results for v_2 (circles) and v_3 (squares) as a function of p_T for inclusive charged hadrons at midrapidity in 0%-5% central ${}^3\text{He}+Au$ collisions at $\sqrt{s_{NN}} = 200$ GeV; error bars are statistical and shaded bars are systematic uncertainties as described in the text. Also shown are various theoretical calculations, see text for details and references.

280 We now compare the experimental data with theory predictions in the literature. Four such predictions shown in
 281 Fig. 4 employ viscous hydrodynamics with η/s at or near the conjectured lower bound $1/4\pi$ [30]. The Glauber+Hydro [31]
 282 (IP-Glasma+Hydro [32]) utilize Glauber (IP-Glasma) initial conditions, and both over predict the magnitude of the v_2
 283 and v_3 data. Improved agreement may be achieved by utilizing a larger value of η/s or by the inclusion of a transition
 284 from QGP to a hadronic cascade, which has much larger viscous effects and thus decreases the overall flow. The SONIC
 285 calculation [14] employs Glauber initial conditions, viscous hydrodynamics, and then at $T = 170$ MeV a transition
 286 to a hadronic cascade. The SUPERSONIC calculation [33] additionally includes pre-equilibrium dynamics that boosts
 287 the initial velocity fields at the earliest times. The impact of pre-equilibrium is modest on the v_2 values and both
 288 calculations agree with the data within uncertainties. The effect of pre-equilibrium on v_3 is significantly larger as the
 289 triangular flow takes longer to develop [14]. The SUPERSONIC prediction agrees well with the experimental data for
 290 $p_T < 1.5$ GeV/ c , and then the data trends towards the SONIC prediction at higher p_T .

291 Lastly, we compare to calculations utilizing the A-Multi-Phase-Transport (AMPT) model [34], which incorporates
 292 both partonic and hadronic scattering, and has recently been compared with anisotropies in central $p+Pb$ and $d+Au$
 293 collisions [35, 36]. AMPT results for ${}^3\text{He}+Au$ agree reasonably with the experimental v_2 and v_3 data for $p_T < 1$ GeV
 294 and then significantly underpredict the data. Possible underlying causes of the anisotropies within the AMPT model
 295 are discussed in Ref. [37].

296 We have presented first results on azimuthal anisotropies v_2 and v_3 in central ${}^3\text{He}+Au$ collisions at $\sqrt{s_{NN}} = 200$ GeV.
 297 Calculations including hydrodynamic expansion of the initial hot spots created in ${}^3\text{He}+Au$ collisions qualitatively de-
 298 scribe the data. Further comparison with different theoretical models should be informative in terms of the contribu-
 299 tions from the initial geometry and each time stage in the medium evolution including pre-equilibrium. Forthcoming
 300 results from $p+Au$ collisions at RHIC will provide a full suite of geometries with highly asymmetric collisions to

301 constrain the origin of the observed anisotropies.

302 We thank the staff of the Collider-Accelerator and Physics Departments at Brookhaven National Laboratory and
 303 the staff of the other PHENIX participating institutions for their vital contributions. We acknowledge support from
 304 the Office of Nuclear Physics in the Office of Science of the Department of Energy, the National Science Foundation,
 305 a sponsored research grant from Renaissance Technologies LLC, Abilene Christian University Research Council,
 306 Research Foundation of SUNY, and Dean of the College of Arts and Sciences, Vanderbilt University (U.S.A), Ministry
 307 of Education, Culture, Sports, Science, and Technology and the Japan Society for the Promotion of Science (Japan),
 308 Conselho Nacional de Desenvolvimento Científico e Tecnológico and Fundação de Amparo à Pesquisa do Estado de
 309 São Paulo (Brazil), Natural Science Foundation of China (P. R. China), Ministry of Science, Education, and Sports
 310 (Croatia), Ministry of Education, Youth and Sports (Czech Republic), Centre National de la Recherche Scientifique,
 311 Commissariat à l'Énergie Atomique, and Institut National de Physique Nucléaire et de Physique des Particules
 312 (France), Bundesministerium für Bildung und Forschung, Deutscher Akademischer Austausch Dienst, and Alexander
 313 von Humboldt Stiftung (Germany), National Science Fund, OTKA, Károly Róbert University College, and the Ch.
 314 Simonyi Fund (Hungary), Department of Atomic Energy and Department of Science and Technology (India), Israel
 315 Science Foundation (Israel), Basic Science Research Program through NRF of the Ministry of Education (Korea),
 316 Physics Department, Lahore University of Management Sciences (Pakistan), Ministry of Education and Science,
 317 Russian Academy of Sciences, Federal Agency of Atomic Energy (Russia), VR and Wallenberg Foundation (Sweden),
 318 the U.S. Civilian Research and Development Foundation for the Independent States of the Former Soviet Union, the
 319 Hungarian American Enterprise Scholarship Fund, and the US-Israel Binational Science Foundation.

320 * Deceased

321 † PHENIX Co-Spokesperson: morrison@bnl.gov

322 ‡ PHENIX Co-Spokesperson: jamie.nagle@colorado.edu

- 323 [1] U. Heinz and R. Snellings, “Collective flow and viscosity in relativistic heavy-ion collisions,” *Ann. Rev. Nucl. Part. Sci.*
 324 **63**, 123 (2013).
- 325 [2] K. Adcox *et al.* (PHENIX Collaboration), “Formation of dense partonic matter in relativistic nucleus-nucleus collisions at
 326 RHIC: Experimental evaluation by the PHENIX Collaboration,” *Nucl. Phys. A* **757**, 184 (2005).
- 327 [3] J. Adams *et al.* (STAR Collaboration), “Experimental and theoretical challenges in the search for the quark gluon plasma:
 328 The STAR Collaboration’s critical assessment of the evidence from RHIC collisions,” *Nucl. Phys. A* **757**, 102 (2005).
- 329 [4] V. Khachatryan *et al.* (CMS Collaboration), “Observation of Long-Range Near-Side Angular Correlations in Proton-Proton
 330 Collisions at the LHC,” *J. High Energy Phys.* **1009**, 091 (2010).
- 331 [5] S. Chatrchyan *et al.* (CMS Collaboration), “Multiplicity and transverse momentum dependence of two- and four-particle
 332 correlations in p Pb and PbPb collisions,” *Phys. Lett. B* **724**, 213 (2013).
- 333 [6] B. B. Abelev *et al.* (ALICE Collaboration), “Long-range angular correlations of π , K , and p in p -Pb collisions at $\sqrt{s_{NN}}=5.02$
 334 TeV,” *Phys. Lett. B* **726**, 164 (2013).
- 335 [7] B. Abelev *et al.* (ALICE Collaboration), “Long-range angular correlations on the near, and away side in p -Pb collisions at
 336 $\sqrt{s_{NN}}=5.02$ TeV,” *Phys. Lett. B* **719**, 29 (2013).
- 337 [8] G. Aad *et al.* (ATLAS Collaboration), “Measurement of long-range pseudorapidity correlations and azimuthal harmonics
 338 in $\sqrt{s_{NN}}=5.02$ TeV proton-lead collisions with the ATLAS detector,” *Phys. Rev. C* **90**, 044906 (2014).
- 339 [9] L. Adamczyk *et al.* (STAR Collaboration), “Long-range pseudorapidity dihadron correlations in d +Au collisions at
 340 $\sqrt{s_{NN}}=200$ GeV,” *Phys. Lett. B* **747**, 265–271 (2015).
- 341 [10] A. Adare *et al.* (PHENIX Collaboration), “Measurement of long-range angular correlation and quadrupole anisotropy of
 342 pions and (anti)protons in central d +Au collisions at $\sqrt{s_{NN}}=200$ GeV,” *Phys. Rev. Lett.* **114**, 192301 (2015).
- 343 [11] A. Adare *et al.* (PHENIX Collaboration), “Quadrupole Anisotropy in Dihadron Azimuthal Correlations in Central d +Au
 344 Collisions at $\sqrt{s_{NN}}=200$ GeV,” *Phys. Rev. Lett.* **111**, 212301 (2013).
- 345 [12] P. Bozek, “Collective flow in p -Pb and d -Pd collisions at TeV energies,” *Phys. Rev. C* **85**, 014911 (2012).
- 346 [13] K. Dusling and R. Venugopalan, “Comparison of the color glass condensate to dihadron correlations in proton-proton and
 347 proton-nucleus collisions,” *Phys. Rev. D* **87**, 094034 (2013).
- 348 [14] J. L. Nagle, A. Adare, S. Beckman, T. Koblesky, J. O. Koop, D. McGlinchey, P. Romatschke, J. Carlson, J. E. Lynn,
 349 and M. McCumber, “Exploiting Intrinsic Triangular Geometry in Relativistic $^3\text{He}+\text{Au}$ Collisions to Disentangle Medium
 350 Properties,” *Phys. Rev. Lett.* **113**, 112301 (2014).
- 351 [15] J.-Y. Ollitrault, “Anisotropy as a signature of transverse collective flow,” *Phys. Rev. D* **46**, 229 (1992).
- 352 [16] K. Adcox *et al.* (PHENIX Collaboration), “PHENIX detector overview,” *Nucl. Instrum. Methods Phys. Res., Sec. A* **499**,
 353 469 (2003).
- 354 [17] K. Adcox *et al.* (PHENIX Collaboration), “PHENIX central arm tracking detectors,” *Nucl. Instrum. Methods Phys. Res.,*
 355 *Sec. A* **499**, 489 (2003).
- 356 [18] A. Adare *et al.* (PHENIX Collaboration), “Centrality categorization for $R_{p(d)+A}$ in high-energy collisions,” *Phys. Rev. C*
 357 **90**, 034902 (2014).

- 358 [19] C. Aidala *et al.*, “The PHENIX Forward Silicon Vertex Detector,” Nucl. Instrum. Methods Phys. Res., Sec. A **755**, 44
359 (2014).
- 360 [20] A. Adare *et al.* (PHENIX Collaboration), “Spectra and ratios of identified particles in Au+Au and d+Au collisions at
361 $\sqrt{s_{NN}}=200$ GeV,” Phys. Rev. C **88**, 024906 (2013).
- 362 [21] A. Adare *et al.* (PHENIX Collaboration), “Suppression of back-to-back hadron pairs at forward rapidity in d+Au Collisions
363 at $\sqrt{s_{NN}}=200$ GeV,” Phys. Rev. Lett. **107**, 172301 (2011).
- 364 [22] A. Adare *et al.* (PHENIX Collaboration), “Nuclear Modification of ψ' , χ_c , and J/ψ Production in d+Au Collisions at
365 $\sqrt{s_{NN}}=200$ GeV,” Phys. Rev. Lett. **111**, 202301 (2013).
- 366 [23] C. Loizides, J. Nagle, and P. Steinberg, “Improved version of the PHOBOS Glauber Monte Carlo,” arXiv:1408.2549.
- 367 [24] M. L. Miller, K. Reygers, S. J. Sanders, and P. Steinberg, “Glauber modeling in high energy nuclear collisions,” Ann.
368 Rev. Nucl. Part. Sci. **57**, 205 (2007).
- 369 [25] A. M. Poskanzer and S.A. Voloshin, “Methods for analyzing anisotropic flow in relativistic nuclear collisions,” Phys. Rev.
370 C **58**, 1671 (1998).
- 371 [26] S. S. Adler *et al.* (PHENIX Collaboration), “Elliptic flow of identified hadrons in Au+Au collisions at $\sqrt{s_{NN}}=200$ GeV,”
372 Phys. Rev. Lett. **91**, 182301 (2003).
- 373 [27] S. S. Adler *et al.* (PHENIX Collaboration), “Measurement of identified π^0 and inclusive photon v_2 and implication to the
374 direct photon production in $\sqrt{s_{NN}}=200$ GeV Au+Au collisions,” Phys. Rev. Lett. **96**, 032302 (2006).
- 375 [28] S. Afanasiev *et al.* (PHENIX Collaboration), “Systematic Studies of Elliptic Flow Measurements in Au+Au Collisions at
376 $\sqrt{s}=200$ GeV,” Phys. Rev. C **80**, 024909 (2009).
- 377 [29] A. J. Baltz, C. Chasman, and S. N. White, “Correlated forward-backward dissociation and neutron spectra as luminosity
378 monitor in heavy ion colliders,” Nucl. Instrum. Methods Phys. Res., Sec. A **417**, 1 (1998).
- 379 [30] P. K. Kovtun, D. T. Son, and A. O. Starinets, “Viscosity in strongly interacting quantum field theories from black hole
380 physics,” Phys. Rev. Lett. **94**, 111601 (2005).
- 381 [31] P. Bozek and W. Broniowski, “Hydrodynamic modeling of ^3He -Au collisions at $\sqrt{s_{NN}}=200$ GeV,” Phys. Lett. B **747**, 135
382 (2015).
- 383 [32] B. Schenke and R. Venugopalan, “Collective effects in light-heavy ion collisions,” Nucl. Phys. A **931**, 1039 (2014).
- 384 [33] P. Romatschke, “Light-Heavy Ion Collisions: A window into pre-equilibrium QCD dynamics?” Eur. Phys. J. C **75**, 305
385 (2015).
- 386 [34] Z.-W. Lin, C. M. Ko, B.-A. Li, B. Zhang, and S. Pal, “A Multi-phase transport model for relativistic heavy ion collisions,”
387 Phys. Rev. C **72**, 064901 (2005).
- 388 [35] A. Bzdak and G.-L. Ma, “Elliptic and triangular flow in p+Pb and peripheral Pb+Pb collisions from parton scatterings,”
389 Phys. Rev. Lett. **113**, 252301 (2014).
- 390 [36] J. D. Orjuela Koop, A. Adare, D. McGlinchey, and J. L. Nagle, “Long-Range Azimuthal Correlations from Parton
391 Scattering in Central p+Au, d+Au, and ^3He +Au Collisions at $\sqrt{s_{NN}}=200$ GeV,” arXiv:1501.06880.
- 392 [37] L. He, T. Edmonds, Z.-W. Lin, F. Liu, D. Molnar, and F. Wang, “Anisotropic parton escape is the dominant source of
393 azimuthal anisotropy from A Multi-Phase Transport,” arXiv:1502.05572.